Stimulated hyper-Raman adiabatic passage. II. Static compensation of dynamic Stark shifts

S. Guérin,* L. P. Yatsenko,† T. Halfmann, B. W. Shore,‡ and K. Bergmann
Fachbereich Physik der Universität, 67653 Kaiserslautern, Germany
(Received 11 May 1998)

When one extends the conventional stimulated Raman adiabatic passage method of population transfer; involving a pump pulse preceded by a Stokes pulse, to situations in which the pump (or pump and Stokes) interaction involves a two-photon transition, there occur unavoidable dynamic Stark shifts which prevent maintenance of the relevant resonance conditions. Such shifts can prevent the desired population transfer. We show, through numerical modeling and analytic considerations, that the detrimental effects of dynamic shifts can be compensated by a suitable choice of (static) detunings of the carrier frequencies of the two pulses, so that population transfer can be achieved. We present simple analytic expressions for bounding the range of detunings for which population transfer can occur, and we present numerical results supporting the simple picture of the two-step linewidth. We illustrate these remarks by considering specific examples. [S1050-2947(98)09311-1]

PACS number(s): 42.50.Hz, 33.80.Be, 42.65.Dr

I. INTRODUCTION

In a companion paper [1] (referred to as paper I) we have presented the basic formalism needed to describe an extension of the technique of stimulated Raman adiabatic passage (STIRAP) [2,3] to a hyper-Raman proces (STIHRAP). The extension can be regarded as a $(2+1)$ or $(2+2)$ rather than a $(1+1)$ process, a notation emphasizing the two-photon character of the interaction [4]. Here we present model studies to explain the reasons for success or failure of population transfer in such schemes.

The conventional STIRAP process for population transfer from state 1 to state 3 makes use of a Stokes pulse (connecting intermediate state 2 with target state 3) followed by a pump pulse (connecting initial state 1 with state 2), each of which induces a single-photon electric-dipole transition. Although the individual pump and Stokes lasers need not be resonant with the associated transitions, it is important that the two carrier frequencies together should maintain two-photon resonance with the overall Raman process.

For the extension considered here, the pump (and/or Stokes) transition is produced by an induced dipole moment, quantified by the product of a polarizability and a pair of electric-field amplitudes (in contrast to the product of a dipole moment and a single field amplitude which characterizes the usual coherent excitation interaction). This hyper-Raman interaction inescapably introduces not only transitions between atomic states (parametrized by generalized multiphoton Rabi frequencies) but also dynamic (Stark) shifts of the atomic energies. Because the shifts vary with time (as established by the pulse shapes), it is generally not possible to maintain resonance conditions between the carrier frequencies of the pulses and the atomic Bohr frequencies. Nevertheless, we demonstrate here with numerical simulation, supported with analytical expressions, that it is possible to achieve the same high degree of population transfer with hyper-Raman STIRAP as can be found with the more customary (single-photon) STIRAP. The key to such success lies in choosing appropriate values for (static) detunings of the lasers.

As we will emphasize, the presence of static detunings implies that successful population transfer takes place via a combination of adiabatic and nonadiabatic time evolution. This requirement stands in contrast to the customary imposition of adiabatic evolution for resonant $(1+1)$ STIRAP, and it requires a more detailed examination of the course of time evolution.

To place the more general problem in context, we first review the simpler conventional STIRAP involving three states, ψ_1, ψ_2, and ψ_3, linked by two successive interactions labeled P (for pump) and S (for Stokes). As is usual, we assume a so-called Λ configuration, wherein the energy of intermediate state ψ_2 lies above that of the other states ψ_1 and ψ_3, but the conclusions hold also for ladder systems. The objective of population transfer is to produce a pulse sequence such that the state vector $\Psi(t)$ has the following behavior:

$$\Psi(t)=\begin{cases}\psi_1 & \text{initially } (t\to-\infty),\\ e^{i\varphi}\psi_3 & \text{finally } (t\to+\infty),\end{cases} \tag{1}$$

where φ is a phase. When the pulses are appropriately timed (Stokes before pump) and simple conditions are fulfilled (two-photon resonance and large pulse area) they can produce complete population transfer from the initial state ψ_1 to the target final state ψ_3.

As noted in paper I, the simplest implementations of this excitation mechanism are described by a rotating-wave approximation (RWA) Hamiltonian whereby each pulse is associated with the Hamiltonian interaction between only one pair of states, as diagrammed in Fig. 1(a) in paper I. We will discuss an extension in which the pump transition is produced by a two-photon transition, as diagrammed in Fig. 1(b)

*Permanent address: Laboratoire de Physique, CNRS, Université de Bourgogne, BP 400, 21011 Dijon, France. Electronic address: guerin@jupiter.u-bourgogne.fr

†Permanent address: Institute of Physics, National Academy of Sciences of Ukraine, Prospekt Nauky 46, Kiev-22, Ukraine.

‡Permanent address: Lawrence Livermore National Laboratory, Livermore, CA 94550.

of paper I or in which both pump and Stokes transitions are by such transitions, as shown in Fig. 1(c) (paper I).

II. THE BASIC (1+1) STIRAP

A. The (1+1) Hamiltonian

Upon defining a pair of single-step laser detunings Δ_P and Δ_S for the carrier frequencies ω_P and ω_S from their assigned Bohr transition frequencies, $\hbar\Delta_P \equiv (E_2-E_1)-\hbar\omega_P$, $\hbar\Delta_S \equiv (E_2-E_3)-\hbar\omega_S$, a two-step detuning $\delta \equiv \Delta_P-\Delta_S$, and the accumulated one-step detuning $\Delta \equiv \Delta_P+\Delta_S$, we can write the basic three-state RWA Hamiltonian matrix as

$$\mathsf{H}(t)=\frac{\hbar}{2}\begin{bmatrix} -\delta & \Omega_P(t) & 0 \\ \Omega_P(t) & \Delta & \Omega_S(t) \\ 0 & \Omega_S(t) & \delta \end{bmatrix}. \tag{2}$$

In conventional STIRAP the parameter δ measures the departure from two-photon resonance. To allow hyper-Raman processes we refer here to δ as a two-step detuning. For the usual STIRAP the Rabi frequencies $\Omega_P(t)$ and $\Omega_S(t)$ are products of dipole moments and electric field envelopes,

$$\begin{aligned} \hbar\Omega_P(t) &= -d_{12}\mathcal{E}_P(t), \\ \hbar\Omega_S(t) &= -d_{32}\mathcal{E}_S(t), \end{aligned} \tag{3}$$

where

$$|\mathcal{E}_P(t)|^2=(2/c\epsilon_0)I_P(t),$$

$$|\mathcal{E}_S(t)|^2=(2/c\epsilon_0)I_S(t).$$

Although it is simplest, and customary, to assume that the laser carrier frequencies are chosen to maintain two-photon resonance, $\delta=0$, such an assumption is inapplicable to the more general hyper-Raman interaction to be considered here. In preparation for the necessity of including nonzero detuning for the more general (2+2) or (2+1) case, we will point out consequences of detuning in the simpler (1+1) case (see [5]).

B. The pulses

The interactions of interest comprise two pulses, the first of which is the Stokes and the second, acting later, is the pump. We take these to have common peak values by writing the pump and Stokes Rabi frequencies as

$$\Omega_S(t)=\Omega_{\max}f(t), \quad \Omega_P(t)=\Omega_{\max}f(t-\tau_P) \tag{4}$$

thereby defining the time delay τ_P of the pump pulse with respect to the earlier Stokes pulse. In what follows, we will require that $f(t)$ has a unit peak value, and we express all elements of the RWA Hamiltonian in terms of the peak Rabi frequency $\Omega_{\max}$.

Because the Rabi frequencies represent pulses, they must vanish at least in the limit of very distant past and future,

$$\Omega_j(-\infty)\to 0, \quad \Omega_j(+\infty)\to 0 \quad (j=P,S). \tag{5}$$

III. ADIABATIC EVOLUTION

The direct numerical integration of the Schrödinger equation with the Hamiltonian of Eq. (2) poses no great difficulty. However, to understand the interplay of parameter choices and population transfer it is necessary to rely on a number of analytic tools related to the notions of adiabatic and diabatic time evolution. The following paragraphs present a consistent set of definitions of the needed tools.

A. Diabatic states

By deleting the off-diagonal elements of any Hamiltonian (the couplings between basis states), one obtains a *diabatic* Hamiltonian, whose (diagonal) elements provide *diabatic energies* $\mu_n(t)$. The basis states themselves provide the eigenvectors of the diabatic Hamiltonian (diabatic states). For the present example, lacking dynamic Stark shifts, the three (constant) diabatic energies and eigenstates are

$$\{\mu_1=-\delta/2,\psi_1\}, \quad \{\mu_2=\Delta,\psi_2\}, \quad \{\mu_3=+\delta/2,\psi_3\}.$$

These are also eigenvalues and eigenstates for the full Hamiltonian before and after the pulse sequence. When the pulses are absent, and there is no degeneracy, the probabilities

$$P_n(t)\equiv|\langle\psi_n|\Psi(t)\rangle|^2 \tag{6}$$

will not change. The objective of the pulse sequence is, starting from the condition $P_1(-\infty)=1$, to make the population transfer efficiency $P_3(\infty)$ as close to unity as possible.

The labels 1, 2, and 3 here identify the original atomic basis states ψ_n, defined such that ψ_1 is the initial state and ψ_3 is the final state. The ordering of the diabatic eigenvalues depends on the values of the detunings. For $\delta>0$, the diabatic energy of ψ_1 lies below that of ψ_3.

B. Adiabatic states

As is evident from the meaning of the acronym STIRAP, adiabatic evolution plays a central role in the STIRAP mechanism for population transfer. However, whereas completely adiabatic evolution offers a satisfactory procedure when there are no dynamic Stark shifts and the resonance condition $\delta=0$ holds, it does not always produce satisfactory population transfer when dynamic shifts occur (see Sec. III C). Thus it is necessary to consider deviations from fully adiabatic evolution.

To describe adiabatic evolution we define, at each time t, a set of (three) eigenstates $\Phi_n(t)$ of the instantaneous RWA Hamiltonian $\mathsf{H}(t)$,

$$[\mathsf{H}(t)-\hbar\varpi_n(t)]\Phi_n(t)=0 \quad (n=1,2,3). \tag{7}$$

These are known as ''dressed states'' or ''adiabatic states,'' and the eigenvalues $\hbar\varpi_n(t)$ are known as ''dressed energies'' or ''adiabatic eigenvalues'' [here $\varpi_n(t)$ denotes a frequency]. It proves useful to refer to the three numerical values as top, middle, and bottom, thereby indicating the ranking in value.

We assign the labels 1, 2, and 3 on dressed states by requiring that initially, prior to the arrival of pulses, the adia-

batic state $\Phi_n(t)$ should coincide with the diabatic state ψ_n, and thereafter the relative order of adiabatic eigenvalues should remain unchanged [i.e., if state ψ_1 has the lowest diabatic energy initially, then at all times the adiabatic state $\Phi_1(t)$ is the state having lowest adiabatic energy]. With this definition, different adiabatic energy curves can touch (be degenerate) but *cannot cross*. We consider smooth pulses, so that a plot of any of the three adiabatic eigenvalues as a function of time will be a continuous curve.

In general, the state vector $\Psi(t)$, which is the solution of a differential equation, is not a single adiabatic state, but it is expressible at any time as some combination of the adiabatic states $\Phi_n(t)$ appropriate to that time t,

$$\Psi(t)=\sum_n B_n(t)\Phi_n(t). \tag{8}$$

In special cases (these are of particular interest) the state vector $\Psi(t)$ may be very nearly a single adiabatic state.

The usefulness of adiabatic states originates from the following property: if at some time t the system is known to be in the adiabatic state $\Phi_n(t)$ associated with the nth eigenvalue, and if the Hamiltonian varies sufficiently slowly and no dressed-state degeneracies occur, then the system will be found at subsequent times in the adiabatic state associated with this same eigenvalue (i.e., the evolution is adiabatic). This property provides a clear prescription for predicting time evolution, and thus plots of eigenvalues versus time are valuable tools for predicting population transfer.

If there occurs a near degeneracy of adiabatic eigenvalues at time t_0, then a given pulse sequence may not be sufficiently slow to allow adiabatic evolution in any small time interval including t_0. In the limit of rapid evolution (or exact degeneracy of adiabatic eigenvalues) the state vector $\Psi(t)$ remains in a fixed superposition of basis states (the evolution is diabatic) at t_0. This necessarily entails a change in the dressed-state composition of $\Psi(t)$ following t_0. When the adiabatic eigenvalues are exactly degenerate, then diabatic evolution past t_0 is guaranteed, with a consequent change in the label of the adiabatic curve associated with $\Psi(t)$ for $t<t_0$ and $t>t_0$.

C. Adiabatic conditions

Complete (or nearly complete) population transfer between basis states can occur in several ways. One possibility is that the evolution be adiabatic at all times. This condition means that the adiabatic eigenvalue $\varpi_1(t)$, which initially (at $t\to-\infty$) coincides with the diabatic eigenvalue $\mu_1=-\delta/2$, must at final times (at $t\to+\infty$) coincide with the diabatic eigenvalue $\mu_3=+\delta/2$. Because adiabatic eigenvalues must maintain a fixed ordering, such a connection is possible only if there is degeneracy of the diabatic energies, i.e., $\delta=0$. Therefore, when static detuning is present ($\delta\neq0$) it is not possible to have good population transfer without some time interval(s) (however brief) during which the evolution is not adiabatic [5,6].

The conditions for adiabatic evolution can be understood from the time-dependent Schrödinger equation expressed in terms of the dressed-state amplitudes $B_n(t)$,

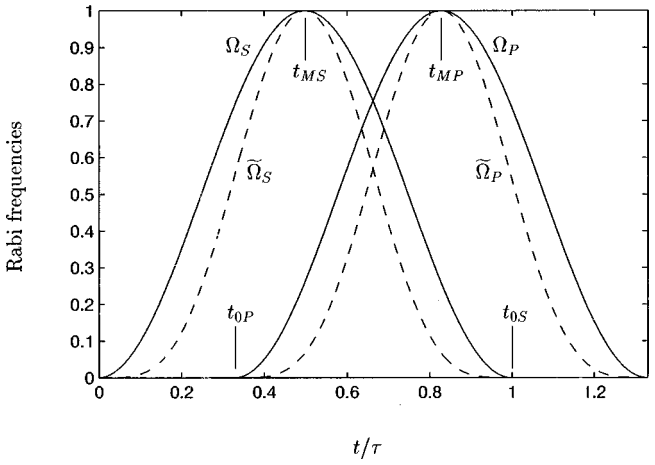

FIG. 1. Relative Rabi frequencies vs time showing Stokes pulse (S) preceding pump pulse (P). Full lines show one-photon Rabi frequencies $\Omega_P(t)$ and $\Omega_S(t)$; dashed lines show two-photon Rabi frequencies $\tilde{\Omega}_P(t)$ and $\tilde{\Omega}_S(t)$. The peak values occur at times t_{MS} and t_{MP}. The pulses overlap between times t_{0P} and t_{0S}.

$$\frac{d}{dt}B_n(t)=-i\varpi_n(t)B_n(t)-\sum_m\left\langle\Phi_n(t)\left|\frac{d}{dt}\Phi_m(t)\right.\right\rangle B_m(t). \tag{9}$$

For the amplitude $B_n(t)$ to remain unchanged in magnitude, it is necessary that the separation of eigenvalue $\varpi_n(t)$ from the nearest values be much larger than any of the off-diagonal diabatic coupling terms $\langle\Phi_n(t)|(d/dt)\Phi_m(t)\rangle$ connected with this dressed state. The adiabatic requirement means, rather roughly, that the pulse areas $A_j\equiv\int_{-\infty}^{\infty}dt\Omega_j(t)$ of pump and Stokes pulses should be much larger than unity, $A_P\gg1$, $A_S\gg1$ [2,8,3].

D. Pulse pairs

To design useful pulse sequences in the presence of dynamic shifts, it is necessary to consider the various possible ways in which the required nonadiabatic interval(s) can occur. The requirements can be seen most clearly if we consider pulses of finite support (i.e., pulses which vanish identically outside a finite time interval). We use half the period of a squared trig function, specifically

$$f(t)=\begin{cases}\sin^2(\pi t/\tau) & \text{for } 0<t<\tau,\\ 0 & \text{otherwise.}\end{cases} \tag{10}$$

This function has the desirable property that the time derivative vanishes at the endpoints (thereby avoiding numerical artifacts associated with abrupt changes). The function $f(t)$ has a pulse area $\int dtf(t)$ equal to $\tau/2$. The full width at half maximum of $f(t)^2$ is 0.364τ. Figure 1 sketches this sequence.

In later sections (see Sec. V) we discuss Rabi frequencies which originate with a two-photon transition. For a given time-dependent intensity profile $I(t)$, the two-photon interaction produces a narrower profile of the pulsed Rabi frequency than does a one-photon interaction. Figure 1 displays this difference.

Although such finite-support pulses are convenient for theoretical analysis, we will also present examples of the commonly assumed Gaussian pulse, and will point out the consequence of having nonzero (albeit small) amplitudes of both pulses at all times.

It proves convenient to denote by t_{0P} the start of the pulse overlap (the instant when the pump pulse begins) and by t_{0S} the cessation of the pulse overlap (when the Stokes pulse terminates). These instants delimit the interval when both pulses act. We denote by t_{MP} and t_{MS} the times when the pump and Stokes pulses, respectively, reach their maximum value (see Fig. 1).

Because the Stokes pulse has no direct action (within the RWA) on the initial state ψ_1, the shape of $\Omega_S(t)$ prior to the arrival of the pump pulse $\Omega_P(t)$ has no effect upon the population which resides there. As long as the Stokes pulse does not violate the conditions which allow the RWA, we need not be concerned with whether the pulse, once started, allows adiabatic evolution: at an infinitesimal time prior to the arrival of the pump pulse, the system is in the initial state ψ_1. Similarly, we need not follow the subsequent time evolution once the Stokes pulse ceases (assuming only that the RWA applies.) If population transfer has occurred, the termination of the Stokes pulse will find the state vector in state ψ_3.

One might guess that satisfactory population transfer would occur if the needed nonadiabatic evolution occurs either prior to or after the interval of pulse overlap, and that during the overlap interval the evolution remained adiabatic. Although this is a useful proposal in the limit of very long interaction times, it is excessively restrictive for pulses of moderate pulse area (say areas as large as several hundred). To treat realistic pulses, it is necessary to allow some nonadiabatic evolution during the pulse overlap.

IV. DETUNING SENSITIVITY OF (1+1) STIRAP

The sensitivity of population transfer to the two-step detuning δ has been analyzed by Danileiko *et al.* [5] to obtain expressions for a two-photon linewidth. Here we extend their ideas, first for the conventional $(1+1)$ STIRAP and then for $(2+2)$ and $(2+1)$ STIHRAP. Initial discussion of the $(1+1)$ process is needed to define the tools used in subsequent analysis, and to demonstrate their use in the simpler case where dynamic Stark shifts are negligible.

When δ vanishes there exists an adiabatic state with the desired property of providing a continuous connection between state ψ_1 and ψ_3. As we shall show, it is possible to achieve good population transfer when δ, though not exactly zero, lies within some bounds (the two-step linewidth lies within these limits [5]). To obtain a simple approximate estimate of the range of parameters for which successful population transfer is possible, we first examine a simple version of the general multilevel ''connectivity'' problem considered by Martin *et al.* [6]. We then modify these results to include dynamic Stark shifts.

A. Semidiabatic eigenvalues

We study the evolution of $\Psi(t)$ by considering separately the action of each laser pulse. For this purpose we define *semidiabatic* Hamiltonians. The Stokes semidiabatic Hamiltonian, $\mathsf{H}^{(S)}(t)$, is constructed by omitting the pump coupling between basis states ψ_1 and ψ_2. The pump semidiabatic Hamiltonian, $\mathsf{H}^{(P)}(t)$, is constructed by omitting the Stokes coupling between basis states ψ_2 and ψ_3. The two semidiabatic Hamiltonians are

$$\mathsf{H}^{(S)}(t)=\frac{\hbar}{2}\begin{bmatrix} -\delta & 0 & 0 \\ 0 & \Delta & \Omega_S(t) \\ 0 & \Omega_S(t) & +\delta \end{bmatrix},$$
$$\mathsf{H}^{(P)}(t)=\frac{\hbar}{2}\begin{bmatrix} -\delta & \Omega_P(t) & 0 \\ \Omega_P(t) & \Delta & 0 \\ 0 & 0 & +\delta \end{bmatrix}. \tag{11}$$

We denote the respective eigenvectors as $\Phi_n^{(S)}(t)$ and $\Phi_n^{(P)}(t)$. It is instructive to consider plots of semidiabatic eigenvalues, obtained by diagonalizing those Hamiltonians. The Stokes semidiabatic eigenvalues, obtained from the expressions

$$2\varpi_1^{(S)}=-\delta, \tag{12a}$$

$$4\varpi_2^{(S)}(t)=\delta+\Delta-\sqrt{|\delta-\Delta|^2+4|\Omega_S(t)|^2}, \tag{12b}$$

$$4\varpi_3^{(S)}(t)=\delta+\Delta+\sqrt{|\delta-\Delta|^2+4|\Omega_S(t)|^2}, \tag{12c}$$

include coupling (by the Stokes interaction) between states ψ_2 and ψ_3. We refer to these semidiabatic curves by the labels $(1S)$, $(2S)$, and $(3S)$. The pump semidiabatic eigenvalues, obtained from the formulas

$$4\varpi_1^{(P)}(t)=-\delta+\Delta-\sqrt{|\delta+\Delta|^2+4|\Omega_P(t)|^2}, \tag{13a}$$

$$4\varpi_2^{(P)}(t)=-\delta+\Delta+\sqrt{|\delta+\Delta|^2+4|\Omega_P(t)|^2}, \tag{13b}$$

$$2\varpi_3^{(P)}=\delta, \tag{13c}$$

include coupling (by the pump interaction) between states ψ_2 and ψ_1. We refer to these semidiabatic curves by the labels $(1P)$, $(2P)$, and $(3P)$.

B. Eigenvalue curves

Figure 2 presents examples of the various eigenvalues plotted against time: Here vertical lines mark the boundaries (t_{0P} and t_{0S}) of the pulse-overlap region. On the left of the adiabatic-eigenvalue diagram, an arrowhead marks state ψ_1, where population initially resides. An arrowhead on the right marks the target state ψ_3. The first row shows Stokes semidiabatic curves, the second row shows pump semidiabatic curves. The lowest row shows adiabatic curves. In each frame the curves bear labels 1, 2, and 3 to identify the asymptotic states to which they correspond. The three columns are distinguished by three different examples of static detunings, as obtained by three choices of carrier frequencies. There are no dynamic Stark shifts present in these cases. Each of the crossings of a semidiabatic eigenvalue has a counterpart in a touching or an avoided crossing of an adiabatic curve.

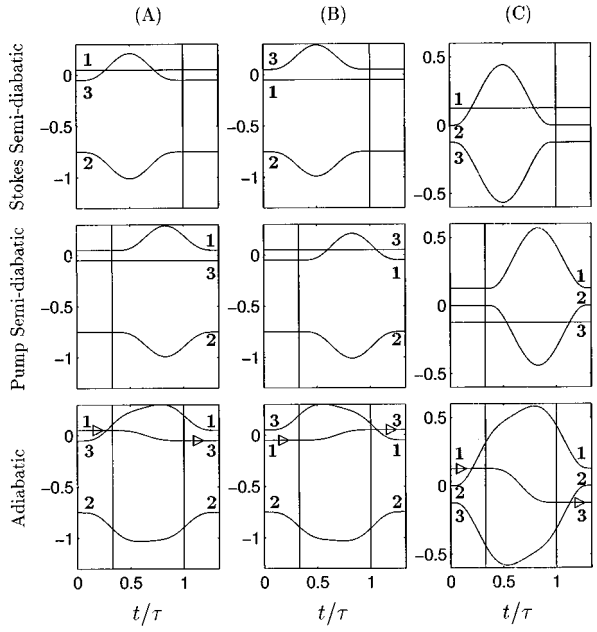

FIG. 2. Examples of eigenvalues (units of $\Omega_{\max}$) vs time (units of τ) for three detunings: (*A*) $\delta=-0.1\Omega_{\max}$, $\Delta=-1.5\Omega_{\max}$, (*B*) $\delta=0.1\Omega_{\max}$, $\Delta=1.5\Omega_{\max}$, and (*C*) $\delta=-0.25\Omega_{\max}$, $\Delta=0$ (note the different ordinate). First row: Stokes semidiabatic curves. Second row: Pump semidiabatic curves. Third row: Adiabatic curves. Numbers on curves show basis state associated with asymptotic eigenvalue. Arrowheads mark the start and end of successful population transfer.

The three examples have been chosen to illustrate three generic possibilities for the diabatic transition needed to achieve the change in the dressed-state composition of $\Psi(t)$ from $\Phi_1(t)$ to $\Phi_3(t)$, as can be seen from the adiabatic curves in the bottom row. For the first column, there occurs an early diabatic transition from $\Phi_1(t)$ to $\Phi_3(t)$. This occurs prior to the arrival of the Stokes pulse. After this crossing, adiabatic evolution carries the system to the desired conclusion, with population in state ψ_3. The second example, in column 2, involves a similar transition $\Phi_1(t)\rightarrow\Phi_3(t)$, but in this case it is at the end of the pulse sequence, when only the pump pulse is present. The third example, in the right-hand column, requires an early dressed-state transition $\Phi_1(t)\rightarrow\Phi_2(t)$ prior to the arrival of the pump pulse, followed by a late transition $\Phi_2(t)\rightarrow\Phi_3(t)$ after the cessation of the Stokes pulse.

Each of these examples shows a process in which a choice of static detuning can make possible successful population transfer. As can be appreciated, different choices of detunings lead to qualitatively different topologies of adiabatic curves, and hence of distinct mechanisms for population transfer. Analysis of generic properties of eigenvalue curves is an important step in determining the range of detunings which will allow population transfer and, when dynamic Stark shifts are present, in selecting suitable static detunings with which to (partially) compensate the otherwise detrimental dynamic shifts.

C. Connectivity

There are several possible approaches to defining the conditions which are conducive to producing good population transfer. One procedure, which we term *full-overlap connectivity*, requires that the evolution be strictly adiabatic during the entire interval of pulse overlap. Although this requirement correctly describes conditions in the limit of pulses of infinite area, it is overly restrictive for pulses of moderate area. A second possibility, which we term *peak-to-peak connectivity*, is less restrictive, and allows intervals of diabatic evolution when both pulses are present: adiabaticity is required only during the time between pulse maxima. Both approaches make use of semidiabatic eigenvalues to suggest bounds on the detunings. The differences between the two criteria become pronounced only when there occur dynamic Stark shifts.

1. Full-overlap connectivity

For pulses of finite support, a given delay time τ_P fixes two particular times: t_{0P} when the pump laser starts, and t_{0S} when the Stokes laser just ceases (see Fig. 1). At these times, the Rabi frequencies have the values $\Omega_{0S}\equiv\Omega_S(t_{0P})$ and $\Omega_{0P}\equiv\Omega_P(t_{0S})$. Between these times both pulses are present, and there can occur no (exact) degeneracies of dressed-state eigenvalues. Thus it is possible, by using pulses of sufficiently large area, to have adiabatic evolution between these two times. By *full-overlap connectivity* we mean that the adiabatic eigenvalue curve which begins (at $t=t_{0P}$) as $(1S)$ later becomes (at $t=t_{0S}$) the curve $(3P)$. To determine the possibility of connecting $(1S)$ with $(3P)$, we must examine (as did the work of Martin *et al.* [6,7]) the ordered relations among the adiabatic eigenvalues at the respective ends of the interval. These are the early semidiabatic eigenvalues $\varpi_n^{(S)}(t_{0P})$ and the late semidiabatic eigenvalues $\varpi_n^{(P)}(t_{0S})$. In the absence of Stark shifts, the desired connectivity occurs only when $(1S)$ and $(3P)$ are the *middle* eigenvalues. These conditions (called *internal connectivity*), taken with Eqs. (12c) and (13c), lead to the following pair of constraints:

$$-\Delta-\sqrt{|\Delta|^2+2|\Omega_{0S}|^2}\leqslant 2\delta\leqslant-\Delta+\sqrt{|\Delta|^2+2|\Omega_{0S}|^2}, \tag{14a}$$

$$+\Delta-\sqrt{|\Delta|^2+2|\Omega_{0P}|^2}\leqslant 2\delta\leqslant+\Delta+\sqrt{|\Delta|^2+2|\Omega_{0P}|^2}. \tag{14b}$$

When static detunings Δ and δ fulfill these conditions, then adiabatic evolution is possible between the state $\Phi_1^{(S)}(t)$ at time t_{0P} and the target state $\Phi_3^{(P)}(t)$ at time t_{0S}. The desired population transfer occurs with the aid of an instantaneous diabatic evolution prior to t_{0P} or after t_{0S}.

In the parameter space defined by axes Δ and δ, the region of full-overlap connectivity is bounded by the four branches of two hyperbolas. When there are no dynamic Stark shifts, the boundaries are, as can be deduced from Eq. (14),

$$\Delta=-\delta+\frac{|\Omega_{0S}|^2}{2\delta}\quad(\text{using}\ \ t=t_{0S}) \tag{15a}$$

for the Stokes curve $\mathcal{F}^{(S)}$,

$$\Delta=\delta-\frac{|\Omega_{0P}|^2}{2\delta}\quad(\text{using}\ \ t=t_{0P}) \tag{15b}$$

for the pump curve $\mathcal{F}^{(P)}$.

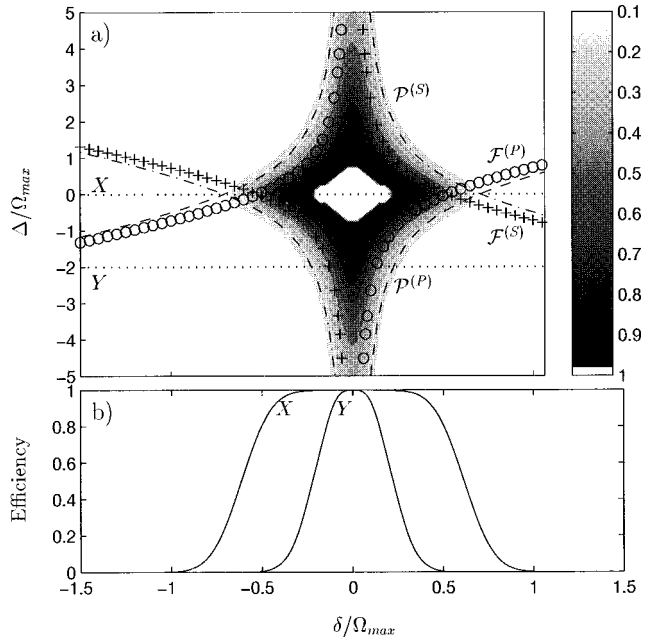

FIG. 3. (a) Connectivity hyperbolas bounding regions of connectivity for $(1+1)$ STIRAP (no dynamic Stark shifts) as a function of two-step detuning δ and one-step detuning Δ (detunings in units of peak Rabi frequency $\Omega_{\max}$). Dashed lines: peak-to-peak connectivity hyperbola $\mathcal{P}^{(P)}$ for pump; dot-dashed lines: peak-to-peak connectivity hyperbola $\mathcal{P}^{(S)}$ for Stokes; circles: full-overlap connectivity hyperbola $\mathcal{F}^{(P)}$ for pump; plus marks: full-overlap connectivity hyperbola $\mathcal{F}^{(S)}$ for Stokes. The hyperbolas are shown together with contours of constant transfer efficiency $P_3(\infty)$ as a function of two-step detuning δ and one-step detuning Δ, obtained by numerical solution of the Schrödinger equation. The numerical simulations are produced for a large pulse area $\Omega_{\max}\tau=100$ and for the delay $\tau_d=33$. Note that efficiencies above 98% are in white. Dotted lines X and Y mark slices plotted in frame (c). (b) Transfer efficiency $P_3(\infty)$ vs normalized two-step detuning $\delta/\Omega_{\max}$ for $\Delta=0$ (X) and $\delta/\Omega_{\max}=-2.0$ (Y), see dotted lines in frame (a).

The conditions that $(1S)$ and $(3P)$ be middle eigenvalues at the ends of the pulse overlap interval mean that adiabatic connectivity occurs within the region bounded by the hyperbolas of Eq. (15). Figure 3 displays these hyperbolas.

2. Peak-to-peak connectivity

With pulses of finite support it is often found that the best population transfer occurs when the start of the pump pulse, at $t=t_{0P}$, occurs slightly before the moment of peak Stokes pulse, at $t=t_{MS}$, and the Stokes pulse terminates after the pump pulse reaches its peak value. With such pulse timings there occur early and late intervals when one pulse is weak, during which the needed nonadiabatic evolution can occur.

The requirement for strictly adiabatic evolution during the entire overlap interval (t_{0P},t_{0S}) thus turns out to be more restrictive than is needed, and we therefore consider a smaller time interval. If there is to occur an intersection of Stokes semidiabatic curves (a necessity if there is to be a diabatic interval prior to the start of the pump pulse), then this must occur no later than the moment when the Stokes pulse is largest. Similarly, if there is to occur a crossing of pump semidiabatic curves (for diabatic evolution after the end of the Stokes pulse), then this must occur no earlier than the moment when the pump pulse is largest. We are thus led to require that strict adiabatic evolution occurs between the time t_{MS} of the maximum Stokes pulse and the time t_{MP} of the maximum pump pulse, and that there should be an adiabatic connection (*peak-to-peak connectivity*) between the dressed states which asymptotically become states ψ_1 and ψ_3. We will show that good population transfer can occur under these less severe requirements. Although the two criteria are similar for $(1+1)$ STIRAP, the distinction becomes significant for $(2+1)$ STIHRAP, as we will see.

The peak-to-peak connectivity region is bounded by branches of the hyperbolas,

$$\Delta=-\delta+\frac{|\Omega_{\max}|^2}{2\delta} \quad (\text{using } t=t_{MS}) \tag{16a}$$

for the Stokes curve $\mathcal{P}^{(S)}$,

$$\Delta=\delta-\frac{|\Omega_{\max}|^2}{2\delta} \quad (\text{using } t=t_{MP}) \tag{16b}$$

for the pump curve $\mathcal{P}^{(P)}$. Within this region, even modest pulse areas may suffice to maintain adiabatic evolution. The needed interval of non- adiabatic evolution is now allowed to occur when both pulses are present (but one is weak).

Figure 3(a) shows the region bounded by the hyperbolas of Eqs. (16). For comparison, it also shows the hyperbolas of Eqs. (15), for $\tau=100$ and $\tau_P=0.33\tau$. The two hyperbolas are quite close (they would be identical if $\tau_P=0.5\tau$). As can be seen from Eq. (16b), limiting cases of the bounding curves are

$$\text{the bound of } |2\delta| \text{ is } |\Omega_{\max}| \quad \text{for } |\Delta|\to 0,$$

$$\text{the bound of } |2\delta| \text{ is } |\Omega_{\max}|^2/\Delta \quad \text{for } |\Delta|\to\infty.$$

It can be seen (and is intuitively obvious) that the largest range of two-step detunings δ occurs when $\Delta=0$, meaning that $\Delta_P=-\Delta_S$. The range of δ which gives good transfer then is set by $\Omega_{\max}$ (i.e., transfer is affected by single-step power broadening). When two-step detuning δ is zero, then any single-step detuning Δ allows an adiabatic connection. Conversely, for large single-step detunings (of the same signs), population transfer is only possible when δ is very close to zero.

D. Choosing the delay

The choice of delay is important for minimizing the power of the lasers needed to achieve complete population transfer for given detunings. In order to have the largest separation between adiabatic eigenvalues, and hence the best chance for adiabatic evolution, this delay should be as small as possible. However, this need for strong coupling among basis states is balanced by the need to have an interval of diabatic evolution at the start or end of the pulse-overlap interval (i.e., close to the beginning for the Stokes semidiabatic diagram and close to the end for the pump semidiabatic diagram).

When the delay is half the pulse length, then the times of pulse maxima coincide with the start or end of the pulse overlap, $t_{0P}=t_{MS}$ and $t_{0S}=t_{MP}$. There is then no distinction

between the two criteria we have proposed for establishing intervals of adiabatic evolution. Shorter delay will improve the transfer efficiency for a given pulse area and peak value. We find, from numerical simulation with pulse areas of $\Omega_{\max}\tau/2=50$, that the largest two-step width for a given power is obtained for delay in the range of approximately 0.3 to 0.4 of the pulse length. We also find that, for any delay in the range of 0.3 to 0.4 of the pulse length, the hyperbolas of the peak-to-peak connectivity always give satisfactory boundaries for population transfer, in the sense that for detuning values outside this connectivity region there is little likelihood of population transfer, and that the highest population transfer occurs for detunings within this region.

E. Numerical results

Given reliable values for atomic parameters (dipole moments and polarizabilities) and pulses, it is, in principle, a straightforward procedure to obtain numerical solutions to the time-dependent Schrödinger equation. By producing many such numerical solutions for a range of the static detunings Δ and δ, one can view the general dependence of population transfer upon these controllable parameters.

Figure 3(a) presents an example of this dependence, shown as a set of contour lines of constant population transfer $P_3(\infty)$ in the parameter space of Δ and δ. These numerical simulations use the sine-squared pulses of Eq. (10) with pulse areas $\Omega_{\max}\tau/2=50$ and delay $\tau_P=\tau/3$. As would be expected, population transfer is high along a ridge (in parameter space) where two-photon resonance occurs, $\delta=0$. For any δ, the highest population transfer occurs for the choice $\Delta=0$, making first-step detuning resonant. As can be seen, the contours follow closely the various hyperbolas, either those deduced from the requirement of full-interval connectivity, Eq. (15), or those deduced from the requirement of peak-to-peak connectivity, Eq. (16). The former give slightly tighter bounds on the detunings. (As will be noted, the two sets of hyperbolas have greater differences when there are dynamic Stark shifts present.)

The bottom frame Fig. 3(b) shows plots of transfer efficiency $P_3(\infty)$ vs two-step detuning δ, for two choices of Δ. The two-photon linewidth, defined as the full width at half maximum of such a curve, lies within the bounds given by the hyperbolas.

The results presented in this figure are for the pulse area of 50. As the area grows larger, the contours become steeper. In the limit of infinite pulse area the full-overlap parabolas serve as the boundaries between transfer efficiencies of unity (within the enclosed region) and zero.

F. Power broadening

The connectivity area has been plotted for normalized variables, detunings divided by the peak Rabi frequency $\Omega_{\max}$. This means, for example, that a doubling of the peak Rabi frequency (by increasing the laser power) will double the range of detunings which will produce a given population transfer. When there are no dynamic Stark shifts, so that the best population transfer occurs for the resonance condition $\delta=0$, the increased range of δ can be understood as power broadening of the two-photon linewidth. However, when there are dynamic shifts, and one overcomes these by static detunings, then a doubling of peak Rabi frequency also doubles the two required static detunings needed to produce the best population transfer. In such cases the notion of a two-photon linewidth loses usefulness.

V. THE HYPER-RAMAN STIHRAP

We study here the extension of STIRAP in which one (or both) Rabi frequency is produced by a two-photon transition, as described in paper I. We will show that although the conventional $(1+1)$ STIRAP process achieves the highest transfer efficiency when the two-step resonance condition $\delta=0$ holds, this choice is not the best when dynamic Stark shifts are present, as is inevitable with a hyper-Raman process (STIHRAP).

A. The (2+2) Hamiltonian

As discussed in paper I, the RWA Hamiltonian for the hyper-Raman $(2+2)$ STIHRAP can be written

$$\mathsf{H}(t)=\frac{\hbar}{2}\begin{bmatrix} -\tilde{\delta}(t) & \tilde{\Omega}_P(t) & 0 \\ \tilde{\Omega}_P(t) & \tilde{\Delta}_P(t)+\tilde{\Delta}_S(t) & \tilde{\Omega}_S(t) \\ 0 & \tilde{\Omega}_S(t) & \tilde{\delta}(t) \end{bmatrix}. \quad (17)$$

In place of the simple product of dipole and field amplitudes that characterizes the interactions of basic STIRAP, the two-photon Rabi frequency requires the product of a polarizability matrix element and a pair of field amplitudes [i.e., the intensity $I_P(t)$]. For linear polarization (along the z axis) the formulas read

$$\hbar\tilde{\Omega}_P(t)=-\frac{1}{2c\epsilon_0}\langle 1|\alpha_{zz}(\omega_P)|2\rangle I_P(t),$$
$$\hbar\tilde{\Omega}_S(t)=-\frac{1}{2c\epsilon_0}\langle 2|\alpha_{zz}(\omega_S)|3\rangle I_S(t). \quad (18)$$

Note that because the interaction is proportional to the square of the electric field amplitude, the associated Rabi frequency has a more sharply peaked pulse shape than is the case for ordinary STIRAP (Rabi frequencies have narrower widths for the given peak value; see Fig. 1).

The definition of the static detunings becomes that of a two-photon transition

$$\hbar\Delta_P\equiv(E_2-E_1)-2\hbar\omega_P, \quad \hbar\Delta_S\equiv(E_2-E_3)-2\hbar\omega_S. \quad (19)$$

In place of the static diagonal elements of the RWA Hamiltonian, there now occur dynamically shifted single-step detunings

$$\tilde{\Delta}_P(t)=\Delta_P+[S_{2S}(t)+S_{2P}(t)]-[S_{1S}(t)+S_{1P}(t)], \quad (20)$$

$$\tilde{\Delta}_S(t)=\Delta_S+[S_{2S}(t)+S_{2P}(t)]-[S_{3S}(t)+S_{3P}(t)] \quad (21)$$

and a dynamically shifted two-step detuning

$$\tilde{\delta}(t)=\Delta_P-\Delta_S+[S_{3S}(t)+S_{3P}(t)]-[S_{1S}(t)+S_{1P}(t)]. \tag{22}$$

Like the two-photon Rabi frequency, the dynamic shifts are proportional to the product of an atomic polarizability and a field intensity. When computing shifts it is important to consider the effect of *each* field upon *each* transition, i.e., both the Stokes laser and the pump laser cause shifts of both the initial and final level. We denote the shift in energy of state i caused by pulse a at time t as $\hbar S_{ia}(t)$. This shift can be computed from appropriate components $\alpha_{zz}(\omega)$ of the frequency-dependent polarizability tensor and the intensity,

$$\hbar S_{ia}(t)=-\frac{1}{2c\epsilon_0}\langle i|\alpha_{zz}(\omega_a)|i\rangle I_a(t)$$

$$(a=P,S;i=1,2,3). \tag{23}$$

Figure 1(c) of paper I diagrams the relevant transitions for $(2+2)$ STIHRAP.

The hyper-Raman Hamiltonian matrix has the same formal expression as the matrix (2) for $(1+1)$ STIRAP. It is only necessary to make the substitutions $\Delta\rightarrow\Delta+s_a^{(\Delta)}(t)$ and $\delta\rightarrow\delta+s_a^{(\delta)}(t)$ where the dynamic shifts are collected into two terms (here a is either S or P),

$$s_a^{(\Delta)}(t)=[S_{1a}(t)-S_{2a}(t)]+[S_{3a}(t)-S_{2a}(t)],$$
$$s_a^{(\delta)}(t)=S_{1a}(t)-S_{3a}(t). \tag{24}$$

The influence of the dynamic Stark shifts is studied by using the same tools as developed in Sec. IV.

B. The (2+1) Hamiltonian

In paper I we considered examples of hyper-Raman STIHRAP in which the pump transition takes place via a two-photon transition, but the Stokes interaction remains the conventional one-photon transition [see Fig. 1(b) in paper I]. The resulting $(2+1)$ hyper-Raman RWA Hamiltonian can be written

$$\mathsf{H}(t)=\frac{\hbar}{2}\begin{bmatrix}-\tilde{\delta}(t) & \tilde{\Omega}_P(t) & 0\\ \tilde{\Omega}_P(t) & \tilde{\Delta}_P(t)+\tilde{\Delta}_S(t) & \Omega_S(t)\\ 0 & \Omega_S(t) & \tilde{\delta}(t)\end{bmatrix}. \tag{25}$$

This expression is a variant of Eq. (17), but with $\Omega_S(t)$ in place of $\tilde{\Omega}_S(t)$ and with dynamic detunings defined as

$$\tilde{\Delta}_P(t)=\Delta_P+S_{2P}(t)-S_{1P}(t), \tag{26}$$

$$\tilde{\Delta}_S(t)=\Delta_S+S_{2P}(t)-S_{3P}(t) \tag{27}$$

with $\hbar\Delta_S=E_2-E_3-\hbar\omega_S$ and $\hbar\Delta_P=E_2-E_1-2\hbar\omega_P$. Thus the dynamic Stark shifts are induced only by the pump field (through the two-photon process), meaning that we set $s_S^{(\delta)}(t)\equiv s_S^{(\Delta)}(t)\equiv 0$. This is the Hamiltonian we shall use in numerical examples.

VI. DETUNING SENSITIVITY OF HYPER-RAMAN STIHRAP

A. Connectivity regions

As in Sec. IV, we analyze the system with the semidiabatic eigenvalues, first when only the Stokes laser acts, and second when only the pump laser acts. The region of full-overlap connectivity is bounded by the four branches of two hyperbolas, which now read

$$\Delta-s_S^{(\Delta)}=-(\delta-s_S^{(\delta)})+\frac{|\Omega_{0S}|^2}{2(\delta-s_S^{(\delta)})}\quad(\text{using } t=t_{0P}) \tag{28a}$$

for the Stokes curve $\tilde{\mathcal{F}}^{(S)}$,

$$\Delta-s_P^{(\Delta)}=(\delta-s_P^{(\delta)})-\frac{|\Omega_{0S}|^2}{2(\delta-s_P^{(\delta)})}\quad(\text{using } t=t_{0S}) \tag{28b}$$

for the pump curve $\tilde{\mathcal{F}}^{(P)}$. The regions of peak-to-peak connectivity are now defined by the hyperbolas

$$\Delta-s_S^{(\Delta)}=-(\delta-s_S^{(\delta)})+\frac{|\Omega_{\max}|^2}{2(\delta-s_S^{(\delta)})}\quad(\text{using } t=t_{MS}) \tag{29a}$$

for the Stokes curve $\tilde{\mathcal{P}}^{(S)}$,

$$\Delta-s_P^{(\Delta)}=(\delta-s_P^{(\delta)})-\frac{|\Omega_{\max}|^2}{2(\delta-s_P^{(\delta)})}\quad(\text{using } t=t_{MP}) \tag{29b}$$

for the pump curve $\tilde{\mathcal{P}}^{(P)}$. Because the Hamiltonian (25) is unchanged, apart from an irrelevant sign, under the transformation (here $a=S,P$)

$$s_a^{(\delta)}\rightarrow-s_a^{(\delta)},\quad s_a^{(\Delta)}\rightarrow-s_a^{(\Delta)},\quad \Delta\rightarrow-\Delta,\quad \delta\rightarrow-\delta, \tag{30}$$

the study of all the generic situations is reduced to the study of the cases involving positive $s_a^{(\delta)}$ and positive $s_a^{(\Delta)}$ (same-sign shifts) or positive $s^{(\delta)}$ and negative $s_a^{(\Delta)}$ (opposing-sign shifts). The cases $s_a^{(\delta)}<0$ are deduced from the previous ones by applying the transformation $s_a^{(\Delta)}\rightarrow-s_a^{(\Delta)}$, $\Delta\rightarrow-\Delta$, and $\delta\rightarrow-\delta$.

The effect of the dynamic Stark shifts, entering the equations as values of $s_a^{(\Delta)}(t)$ and $s_a^{(\delta)}(t)$ at specific times, is to offset the hyperbolas from the positions they occupy in the absence of dynamic shifts. When the hyperbolas are offset in this way, there occur new options for connectivity. Specifically, in addition to the internal semidiabatic connectivity already described for the $(1+1)$ STIRAP, it becomes possible to have semidiabatic connectivity if the eigenvalues $\varpi_1^{(S)}$ and $\varpi_3^{(P)}$ are either the top or the bottom values. There are two possibilities for such an *external connectivity region*. First, curves $(S1)$ at $t=t_{MS}$ and $(P3)$ at $t=t_{MP}$ are each the bottom eigenvalues. This condition is satisfied in a parameter region defined by the intersection of the right outside of the Stokes hyperbola $\tilde{\mathcal{P}}^{(S)}$ with the left outside of the pump hyperbola $\tilde{\mathcal{P}}^{(P)}$. Alternatively, curves $(S1)$ at $t=t_{MS}$ and

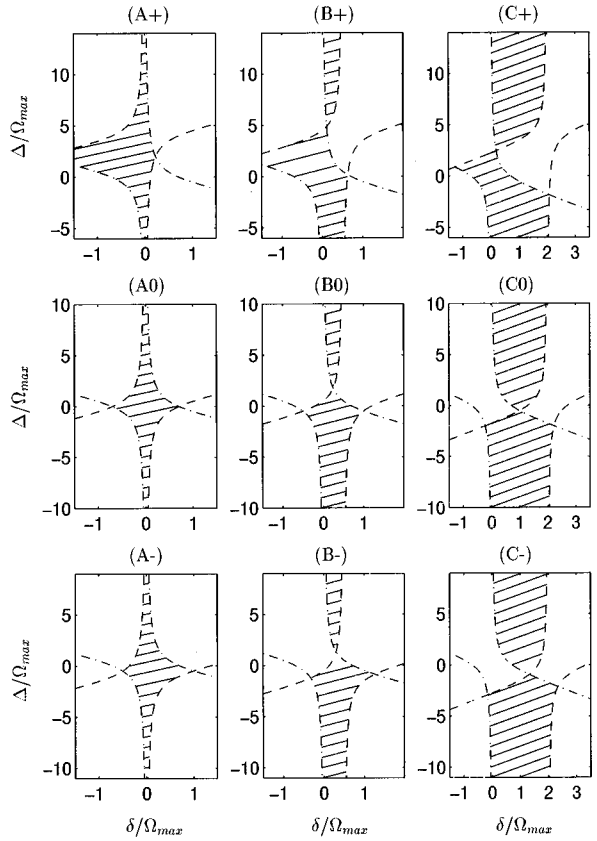

FIG. 4. Connectivity hyperbolas and regions (hashed) of peak-to-peak connectivity for $(2+1)$ STIHRAP (with dynamic Stark shifts) as a function of two-step detuning δ and one-step detuning Δ (detunings in units of peak Rabi frequency $\Omega_{\max}$). The various frames differ in the Stark shifts $s^{(\Delta)}$ and $s^{(\delta)}$. The column label (A) holds for $s^{(\delta)}=0$, (B) for $s^{(\delta)}=0.5\Omega_{\max}$, and (C) for $s^{(\delta)}=2\Omega_{\max}$; the row label (0) holds for $s^{(\Delta)}=0$, $(-)$ for $s^{(\Delta)}=-\Omega_{\max}$, and $(+)$ for $s^{(\Delta)}=4\Omega_{\max}$.

$(P3)$ at $t=t_{MP}$ are each the top eigenvalues. This condition means the intersection of the left outside of the Stokes hyperbola with the right outside of the pump hyperbola. Note that for given Stark shifts, neither of these conditions can hold for the same set of parameters (i.e., on the same diagram). It is significant that the two-step resonance condition $\delta=0$ never permits adiabatic connectivity with these external-connectivity conditions.

Figure 4 shows examples of the connectivity regions (hashed areas) defined by the semidiabatic hyperbolas, for several choices of the dynamic Stark shifts of $(2+1)$ STIRAP. We assume that shifts arise only from the pump pulse, and we denote $s^{(\delta)}\equiv s_P^{(\delta)}$, $s^{(\Delta)}\equiv s_P^{(\Delta)}$.

Frame $(A0)$, center left, repeats the case of Fig. 3, where the Stark shifts are negligible. The columns (A), (B), and (C) take increasing values of the shift parameter $s^{(\delta)}$, while the rows $(+)$, (0), and $(-)$ take positive, null, and negative values for the shift parameter $s^{(\Delta)}$. In the top row the Stark shifts $s^{(\delta)}$ and $s^{(\Delta)}$ have the same signs, while in the bottom row the two shifts have opposite signs. Table I gives explicit values.

TABLE I. Values of the Stark shifts $(s^{(\Delta)},s^{(\delta)})$ in units of $\Omega_{\max}$ for Fig. 4.

	A	*B*	*C*
$(+)$	(4,0)	(4,0.5)	(4,2)
(0)	(0,0)	(0,0.5)	(0,2)
$(-)$	$(-1,0)$	$(-1,0.5)$	$(-1,2)$

As can be seen, the presence of dynamic Stark shifts causes the bounded region to separate into two nonoverlapping regions, one including large positive values of Δ and the other including large negative values. There is no symmetry between positive and negative Δ, nor is the border exactly at $\Delta=0$. For any $s^{(\delta)}$ the widths of the hashed regions increase with increasing shift $s^{(\Delta)}$.

In presenting Fig. 4, we have assumed that shifts arise only from the pump pulse. The graph can be used also when the shifts are induced by the Stokes pulse, after making the transformation $\delta\rightarrow-\delta$ and $s^{(\delta)}\rightarrow-s_S^{(\delta)}$. That is, one must reflect the individual frames around $\delta=0$ (and consider then $s_S^{(\delta)}<0$).

For the $(2+2)$ STIHRAP, shifts can arise from both pump and Stokes pulses. This produces the same frames of Fig. 4 in the new coordinate system $\delta\rightarrow\delta+s_S^{(\delta)}$ and $\Delta\rightarrow\Delta+s_S^{(\Delta)}$, the relative shifts for the pump hyperbolas becoming $(s_P^{(\delta)}-s_S^{(\delta)},\ s_P^{(\Delta)}-s_S^{(\Delta)})$ in this coordinate system.

B. Stark compensation

The occurrence of dynamic Stark shifts produces time-dependent two-step detunings which make population transfer difficult. It is possible to choose static detunings which overcome the deleterious effects of the dynamic detunings. In that sense, the static shifts provide a partial compensation for the dynamic Stark shifts.

It is instructive to rewrite the conditions of internal connectivity [bounded by the four branches of hyperbolas (29)] as

$$(S_{3S}-S_{1S}+\delta)1\left(S_{2S}-S_{1S}+\frac{\delta+\Delta}{2}\right)<\frac{|\Omega_{\max}|^2}{4}$$

$$(\text{using } t=t_{MS}), \quad (31a)$$

$$(S_{3P}-S_{1P}+\delta)\left(S_{3P}-S_{2P}+\frac{\delta-\Delta}{2}\right)<\frac{|\Omega_{\max}|^2}{4}$$

$$(\text{using } t=t_{MP}). \quad (31b)$$

We see clearly from these formulas that, to satisfy the conditions of internal connectivity, the static two-step detuning δ can be used to compensate the dynamic Stark shift between the initial and final state, and $\delta\pm\Delta$ can compensate dynamic Stark shifts involving the intermediate level. This is an important result of our analysis: rather than attempt the difficult task of producing a frequency-varying pulse which compensates dynamic Stark shifts at each moment, it is possible to employ detuned constant-frequency pulses.

C. Example: Opposite-sign shifts

In any intended application of hyper-Raman STIHRAP, it is important to obtain reliable estimates of polarizabilities,

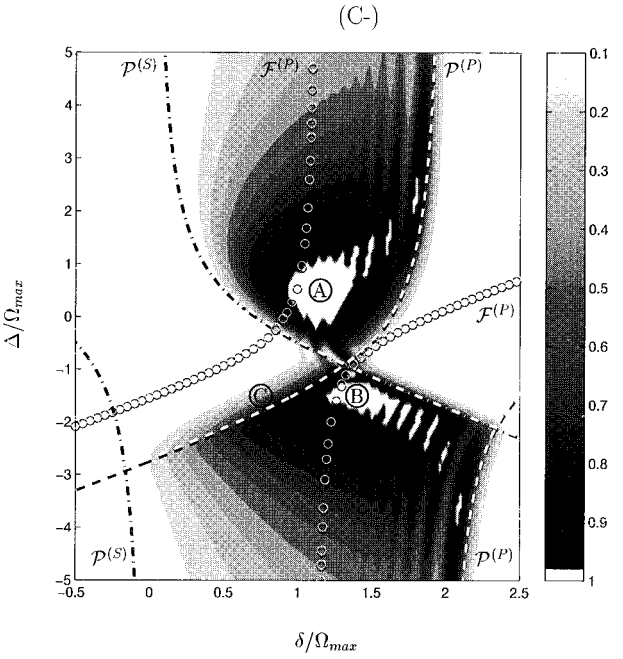

FIG. 5. Contours of constant transfer efficiency $P_3(\infty)$ for varying relative detunings $\Delta/\Omega_{\max}$ and $\delta/\Omega_{\max}$ and the conditions of region $(C-)$ of Fig. 4. Efficiencies above 98% are shown as white. Dashed lines: peak-to-peak connectivity hyperbola $\mathcal{P}^{(P)}$ for pump; dot-dashed lines: peak-to-peak connectivity hyperbola $\mathcal{P}^{(S)}$ for Stokes; circles: full-overlap connectivity hyperbola $\mathcal{F}^{(P)}$ for pump. Points A and B mark parameter values of highest transfer efficiency. Point C marks a third point, for display in Fig. 6.

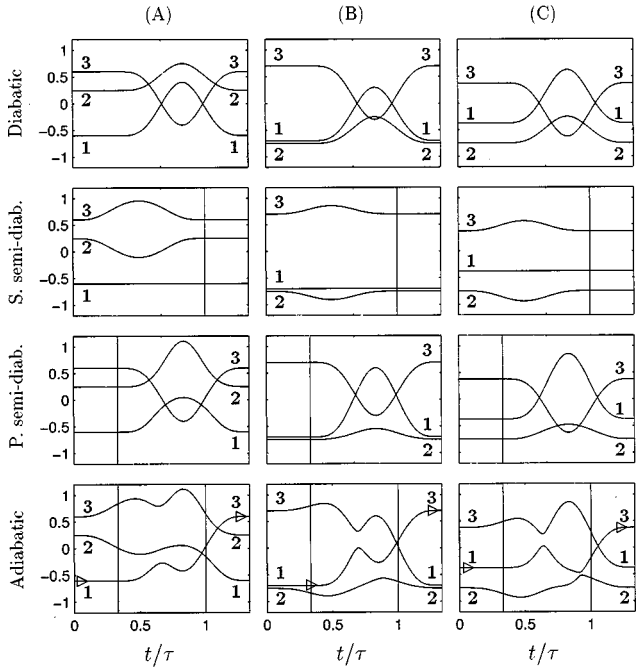

FIG. 6. Eigenvalues (units of $\Omega_{\max}$) vs time (units of τ) for the parameter choices (A), (B), and (C) of Fig. 5. (A) $\Delta=0.5\Omega_{\max}$, $\delta=1.2\Omega_{\max}$; (B) $\Delta=-1.5\Omega_{\max}$, $\delta=1.4\Omega_{\max}$; and (C) $\delta=0.75\Omega_{\max}$, $\Delta=-1.5\Omega_{\max}$. First row: diabatic curves; second row: Stokes-diabatic curves; third row: pump-diabatic curves; bottom row: adiabatic curves. Numbers on curves show basis state associated with an asymptotic eigenvalue. Arrowheads mark the start and end of successful population transfer.

from which one can obtain estimates of two-photon Rabi frequencies and dynamic Stark shifts. To elucidate some of the properties of population transfer, we consider here some simple model examples of Stark shifts. The effects are contained within two parameters $s^{(\delta)}(t)$ and $s^{(\Delta)}(t)$. To study the peak-to-peak connectivity, these parameters are evaluated at the fixed time t_{MP} corresponding to the peak pump pulse. We will then use in the following the convenient notation

$$s^{(\delta)}\equiv s^{(\delta)}(t_{MP}), \quad s^{(\Delta)}\equiv s^{(\Delta)}(t_{MP}). \tag{32}$$

As will be seen, there are important differences between cases when these two parameters have the same sign or opposite signs.

1. Contours

To show the usefulness and relevance of the various connectivity relations, we present examples of numerical solutions to the Schrödinger equation, for various choices of the excitation parameters. We show contour plots of transfer efficiency $P_3(\infty)$ for fixed pulse delay τ_P (and fixed peak value $\Omega_{\max}$) but varying Δ and δ. The plots also display the hyperbolas which bound the region of peak-to-peak connectivity and of full-overlap connectivity.

Figure 5 shows an example of a contour plot of transfer efficiency $P_3(\infty)$ when the Stark shifts $s^{(\delta)}$ and $s^{(\Delta)}$ have opposite signs (here $s^{(\delta)}=2.0\Omega_{\max}$, $s^{(\Delta)}=-1.0\Omega_{\max}$; note that these values are not far from the ones for helium $s^{(\delta)}=1.87\Omega_{\max}$, $s^{(\Delta)}=-1.57\Omega_{\max}$ [1]), as occurs for the frame $(C-)$ of Fig. 4. One readily sees that the contours follow quite well the hyperbolas of peak-to-peak connectivity $\mathcal{P}^{(P)}$ and $\mathcal{P}^{(S)}$: little population transfer occurs when the corresponding constraints are not met. It is clear that the full-overlap connectivity hyperbolas $\mathcal{F}$ are not relevant for bounding the contours. For simplicity we have not plotted the (nonshifted) Stokes full-overlap hyperbola, which is close to the $\mathcal{P}^{(S)}$ curve [as in $(1+1)$ STIRAP].

As expected from the hashed region $(C-)$ of Fig. 4, there occur two disjoint regions of population transfer. There are thus two distinctly different choices for optimal values of δ and Δ. For the upper region, good values (point A) are near $\Delta=0.5\Omega_{\max}$, $\delta=1.2\Omega_{\max}$. For the lower region, good values (point B) are near $\Delta=-1.5\Omega_{\max}$, $\delta=1.4\Omega_{\max}$.

One can see that the region of highest population transfer is well within the predicted region for peak-to-peak connectivity (the hashed regions of Fig. 4).

One can also see that there does occur some population transfer for detuning values which lie outside the peak-to-peak connectivity region. The point labeled C is an example. Although the parameter choices here do not meet the peak-to-peak connectivity criteria, they do still fall within bounds set by full-overlap connectivity.

2. Eigenvalues

It is instructive to examine plots of eigenvalue curves for particular cases of the parameter choices.

Figure 6 shows three examples of time histories of eigenvalues. Columns (A) and (B) are for choices of detunings

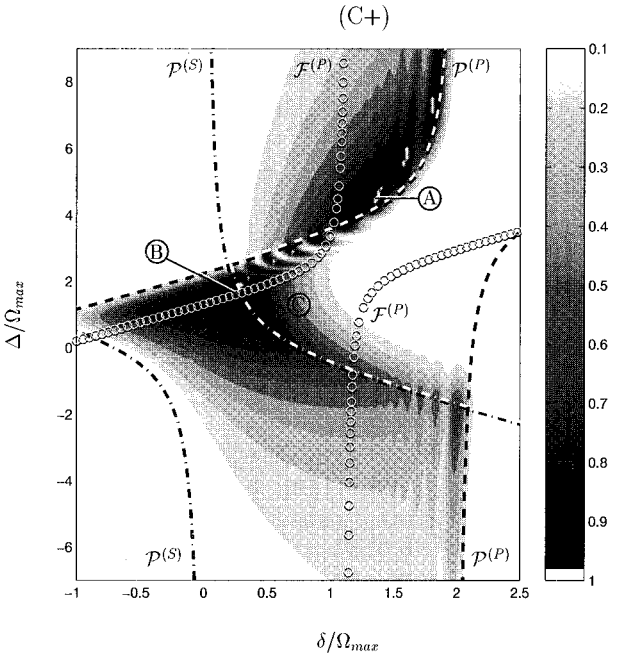

FIG. 7. Contours of constant transfer efficiency for varying Δ and δ as in Fig. 5 but for the conditions of region $(C+)$ of Fig. 4.

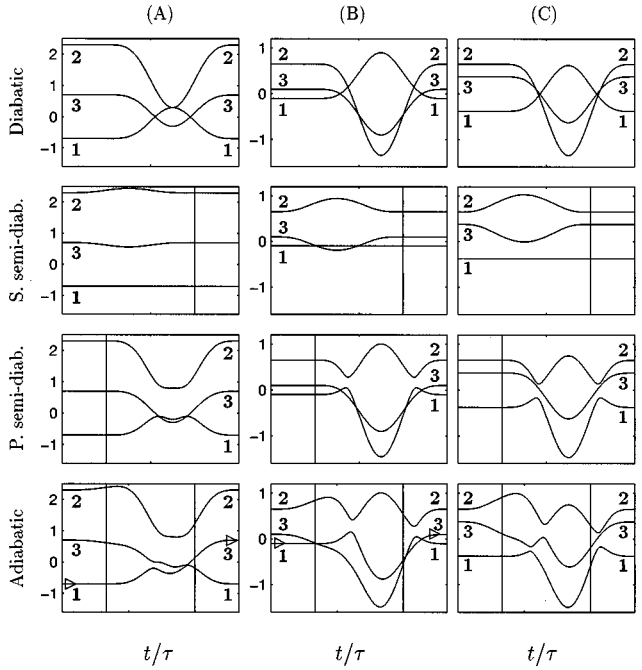

FIG. 8. Eigenvalues vs time, as in Fig. 6, but for parameter choices (A), (B), and (C) of Fig. 7. (A) $\delta=1.35\Omega_{\max}$, $\Delta=4.5\Omega_{\max}$, (B) $\delta=0.2\Omega_{\max}$, $\Delta=1.4\Omega_{\max}$, and (C) $\delta=0.75\Omega_{\max}$, $\Delta=1.3\Omega_{\max}$.

which produce the highest transfer efficiency. (In both cases, we have found numerical efficiency of more than 99%.) The adiabatic curves in column (A) are an example involving diabatic transitions $\Phi_1(t)\rightarrow\Phi_2(t)\rightarrow\Phi_3(t)$, whereas column (B) is a transition $\Phi_1(t)\rightarrow\Phi_3(t)$. In each of these cases there occurs, just before the end of the Stokes pulse, a near degeneracy of eigenvalues. Were the evolution to be adiabatic, population transfer would fail. But because the Stokes pulse is weak at this time, the system evolves diabatically and transfer succeeds.

Column (C) shows an example in which the conditions of adiabatic connectivity are met, yet little transfer occurs (an efficiency of 32% is found). The difficulty here is, again, a near degeneracy when the Stokes pulse is weak. If the evolution were adiabatic, then transfer would be complete. With the given pulse areas, some diabatic coupling occurs between states $\Phi_1(t)$ and $\Phi_2(t)$, and so population transfer is not complete.

D. Example: Same-sign shifts

1. Contours

Figure 7 shows an example of a contour plot of constant transfer efficiency when the Stark shifts $s^{(\delta)}$ and $s^{(\Delta)}$ have the same signs (here $s^{(\delta)}=2.0\Omega_{\max}$, $s^{(\Delta)}=4.0\Omega_{\max}$) as occurs for the frame $(C+)$ of Fig. 4. As with the preceding figure, the contours fit within a region bounded by peak-to-peak hyperbolas, and little population transfer occurs outside these regions. There does exist a residual population transfer (diminishing with distance from the peak-to-peak connectivity hyperbolas) outside the peak-to-peak connectivity boundaries.

There occur two disjoint regions of population transfer. For the upper region, a good choice (point A) for static detunings is near $\Delta=4.5\Omega_{\max}$, $\delta=1.35\Omega_{\max}$. For the lower region, a good choice (point B) is near $\Delta=1.4\Omega_{\max}$, $\delta=0.2\Omega_{\max}$. This latter choice is less sensitive to small variations in detunings, and thus it offers a more robust choice.

Within the region bounded by peak-to-peak connectivity hyperbolas, the contour lines show a clear asymmetry of the dependence of transfer efficiency upon δ. The region bordering (to the left) the hyperbolas $\mathcal{P}^{(P)}$ is favored over regions with smaller δ.

2. Eigenvalues

Figure 8 shows three examples of time histories of eigenvalues.

Column (A) shows an example of high transfer efficiency (99% is found numerically). As can be seen from the adiabatic curves, successful transfer requires that the diabatic evolution $\Phi_1(t)\rightarrow\Phi_3(t)$ occur at near-degeneracy at the end of the Stokes pulse.

Column (B) shows an example of relatively high efficiency (97% is found) which requires three intervals of diabatic evolution, one of which occurs just after the pump pulse begins. The sequence may be viewed as the changes $\Phi_1(t)\rightarrow\Phi_3(t)\rightarrow\Phi_1(t)\rightarrow\Phi_3(t)$.

Column (C) shows an example in which there is no adiabatic connectivity, either full-overlap or peak-to-peak, yet appreciable transfer occurs (41% is found for this example). As can be seen from the adiabatic curves, there occurs a moment of close approach of two adiabatic curves, at which time the lack of completely adiabatic evolution can produce the needed change $\Phi_1(t)\rightarrow\Phi_3(t)$.

E. General observations

As with the $(1+1)$ STIRAP, our numerical simulations of $(2+1)$ STIHRAP suggest that it is best to have delay in the range of 0.3 and 0.4 of the pulse length.

In the limit of infinite pulse area, leading to the absence of diabatic following during the pulse overlap, the good transfer area is bounded by the full-overlap hyperbolas.

Several other features of the contour plot are noteworthy, and are typical of features found for other Stark shifts.

In each example good population transfer is possible only within a limited range of detunings Δ. However, within this range there are values of Δ for which no choice of δ can produce good transfer.

It is also notable that the right-hand portion of the connectivity region shows a pronounced ripple structure. This observation is discussed in more detail in the next section.

VII. OTHER CONSIDERATIONS

A. Regions of interferences

Although the simple notion of connectivity suffices to delimit regions where good population transfer can occur, there are interesting patterns of valleys visible along two of the boundaries (see, for example, Fig. 5). These are regions of parameter space lying between two boundary hyperbolas: those of peak-to-peak and full-overlap connectivity. In such cases there occur a pair of diabatic curve crossings. Successful population transfer requires that the system pass adiabatically through the first interval and diabatically through the second. Figure 10 shows an example of adiabatic eigenvalues exhibiting this possibility. However, the evolution is neither completely adiabatic nor completely diabatic. During the evolution, the basis-state composition of $\Psi(t)$ splits into two parts after the first avoided crossing and these amplitudes interfere when time evolution brings $\Psi(t)$ to the second avoided crossing. The interferences depend on the time between the two avoided crossings, and through this upon δ and Δ.

B. Population in the intermediate state

It is usually desirable to minimize the population which occurs transiently in state ψ_2 during the population transfer. In ordinary $(1+1)$ STIRAP, under the conditions $\delta=0$, such population occurs as a consequence of (unintentional) nonadiabatic evolution, which introduces some dressed states $\Phi_2(t)$ or $\Phi_3(t)$ into the composition of the state vector $\Psi(t)$. When detunings are present, $\delta\neq 0$, even adiabatic evolution of $\Psi_1(t)$ will introduce some contribution to $\Psi(t)$ from basis state ψ_2.

Here we note, for the examples considered above, how the maximum contribution of ψ_2 to $\Psi(t)$ is affected by the choice of static detunings δ and Δ.

Figure 9 shows contours of peak value $P_2(t)$ for the same conditions used in producing Fig. 5.

The peak population in state ψ_2 depends most strongly upon the single-photon detuning Δ, which brings this state into resonance with the (two-photon) pump frequency. The population is relatively insensitive to δ, the two-step detuning.

Unlike the contours of $P_3(\infty)$, these contours of P_2 do not show a population confined within a region bounded by connectivity hyperbolas.

We can give simple analytic expressions which approximately bound parameter regions where appreciable population occurs in state 2 during the process. In a first approximation, we can argue that appreciable population occurs in state 2 during the process when *the pump two-photon energy* $2\omega_P$ *is swept by the time-shifted two-photon resonance* $E_2+S_{2P}(t)-[E_1+S_{1P}(t)]$, i.e., when

$$|\Delta_P|<|S_{1P}(t_{MP})-S_{2P}(t_{MP})|. \tag{33}$$

The previous condition is equivalent to saying that the diabatic curve connected to 1 crosses the one connected to 2. We thus find that the region of high population in level 2 lies between the two lines (see Fig. 9),

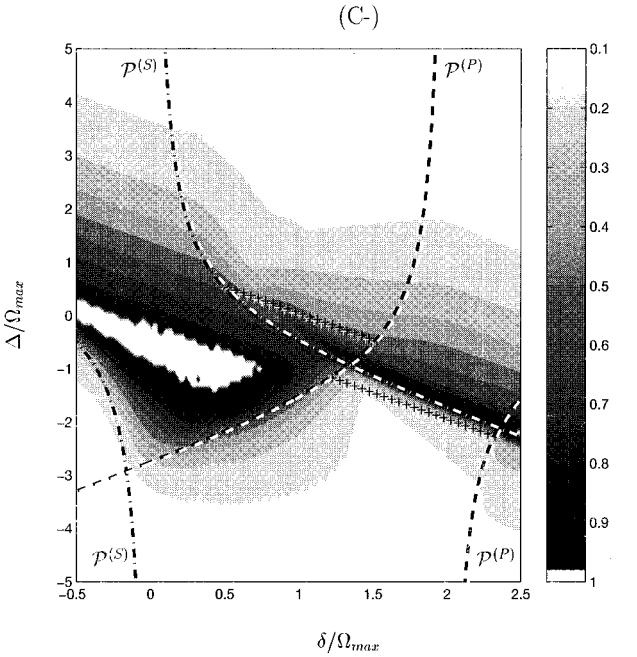

FIG. 9. Contours of constant maximum population $P_2(t)$ during the pulse process, for varying Δ and δ and the conditions of Fig. 5. Dashed lines: peak-to-peak connectivity hyperbola $\mathcal{P}^{(P)}$ for pump; dot-dashed lines: peak-to-peak connectivity hyperbola $\mathcal{P}^{(S)}$ for Stokes. The lines marked with a plus are the bound region of appreciable population $P_2(t)$ during the process.

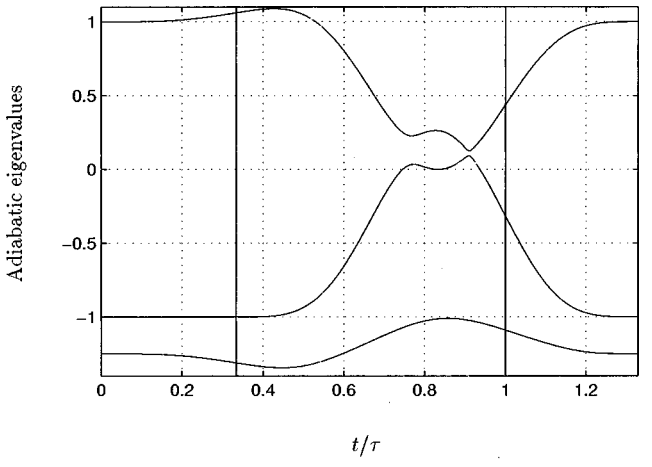

FIG. 10. Adiabatic eigenvalues (units of $\Omega_{\max}$) vs time (units of τ) for $\Delta=-2.5\,\Omega_{\max}$, $\delta=2\,\Omega_{\max}$. At the left-hand avoided crossing, there occurs a splitting of the population in two parts which recombine and interfere at the right-hand avoided crossing.

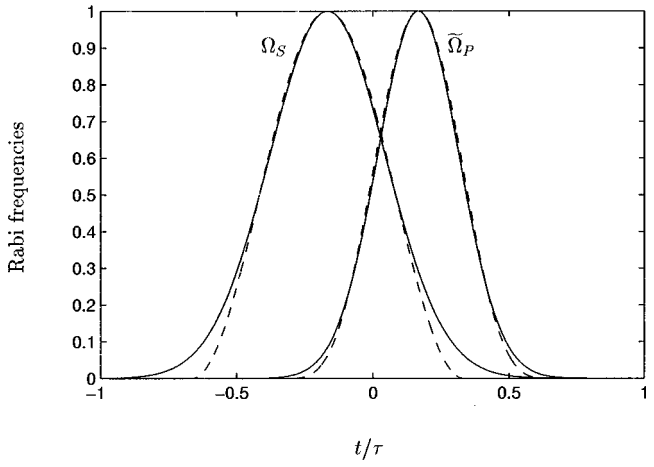

FIG. 11. Rabi frequencies vs time for $(2+1)$ STIHRAP. Full lines are Gaussian pulses, dashed lines are sine-squared pulses.

$$\Delta = -\delta, \tag{34a}$$

$$\Delta = -\delta + [s^{(\delta)}(t_{MP}) + s^{(\Delta)}(t_{MP})]. \tag{34b}$$

We note that this approximation is valid inside the connectivity region, but not in the left-hand outside.

C. Pulse shape effects

The analysis of adiabatic following for pulse pairs is simplest when the pulses have finite temporal support, so that there exists only a limited time during which both pulses act. Gaussian pulses, by contrast, extend indefinitely in time. A comparison of the finite-support sine pulses (used in the preceding analysis) with Gaussian pulses is therefore instructive. We use a Gaussian pulse having the same half-width, 0.5τ, as the sine-squared pulse,

$$f(t) = \exp[-16\ \ln 2(t/\tau)^2]. \tag{35}$$

This pulse is normalized to have area $\int dt f(t) = \tau\sqrt{\pi/16\ \ln 2} \approx 0.53\tau$; the full width at half maximum of $f(t)^2$ is 0.354τ.

Figure 11 shows the two classes of pulses being considered. The full lines show the finite support pulses, the dashed lines show the Gaussian pulses.

Figure 12 shows an example of population transfer efficiency contours. The conditions are those of Fig. 5 except that pulses are Gaussian in shape.

As can be seen, there are choices of Δ and δ which produce high transfer efficiency. However, it is also noteworthy that for a range of parameter choices the process is not so robust as with pulses of finite support: small changes in detuning (or in pulse area) can produce large changes in population transfer. This sensitivity is to be expected from the nature of the curve intersections. In ideal cases there would be an avoided crossing followed by a degeneracy at which diabatic evolution would occur. However, with Gaussian pulses there are never any adiabatic degeneracies, because there is always some finite amplitude of each pulse, and hence diabatic evolution cannot be guaranteed.

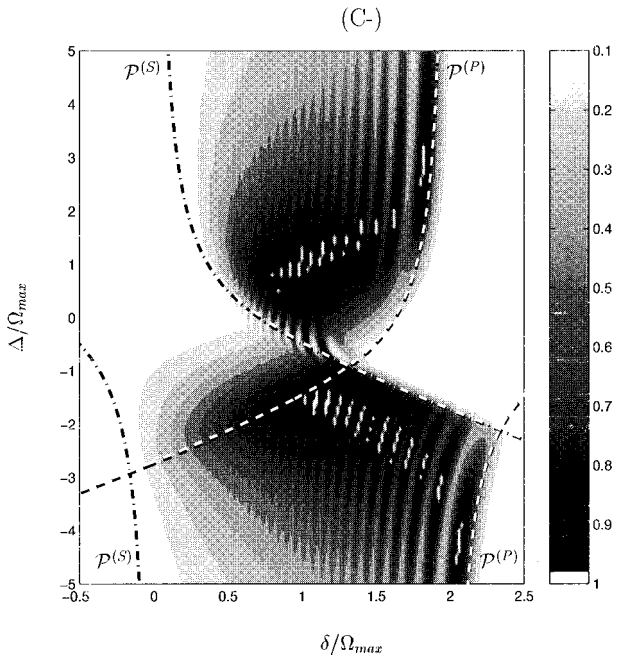

FIG. 12. Contours of constant transfer efficiency as in Fig. 5 but for Gaussian pulses.

VIII. CONCLUSIONS

We have considered coherent population transfer produced by delayed pulses (a generalization of STIRAP) with two-photon coupling between the initial and intermediate states. Although the use of a two-photon transition in place of a one-photon transition introduces few novel mathematical distinctions, the physics of the excitation process can be quite different from conventional STIRAP. Because the two-photon Rabi frequency is, like the dynamic Stark shifts, proportional to intensity and polarizability matrix elements, it is essential to consider the effects of such shifts. They can dramatically alter the possibility for successful population transfer.

We have shown how to choose a (static) detuning from the two-step resonance to reduce the detrimental effect of time-dependent Stark shifts.

We have presented some simple analytic expressions for bounding the range of detunings (one- and two-step) where successful population transfer can occur. Though the notions behind the formulas are very simple (connectivity of adiabatic eigenvalues for a specified time interval), they provide useful approximations, as our numerical modeling demonstrates.

In the present work we have discussed the phenomenology. Clearly, suitable choices for static detunings and pulse delays can only be identified when the relevant polarizabilities are known. Calculations are needed to ascertain the suitability of a given choice of laser parameters.

ACKNOWLEDGMENTS

S.G. thanks the European Union HCM Network ''Laser Controlled Dynamics of Molecular Processes and Applications'' (Grant No. ERB-CHR-XCT-94-0603) and ''La Fon-

dation Carnot'' for support. L.Y. is grateful to the Deutsche Forschungsgemeinschaft for support of his visit to Kaiserslautern. B.W.S. thanks the Alexander von Humboldt Stiftung for their financial support; his work is supported in part under the auspices of the U.S. Department of Energy at Lawrence Livermore National Laboratory under Contract No. W-7405-Eng-48 and by a NATO collaborative research grant.

[1] L. P. Yatsenko, S. Guérin, T. Halfmann, K. Böhmer, B. W. Shore, and K. Bergmann, preceding paper, Phys. Rev. A **58**, 4683 (1998).

[2] U. Gaubatz, P. Rudecki, S. Schiemann, and K. Bergmann, J. Chem. Phys. **92**, 5363 (1990); J. R. Kuklinski, U. Gaubatz, F. T. Hioe, and K. Bergmann, Phys. Rev. A **40**, 6741 (1989); S. Schiemann, A. Kuhn, S. Steuerwald, and K. Bergmann, Phys. Rev. Lett. **71**, 3637 (1993).

[3] B. W. Shore and K. Bergmann, in *Molecular Dynamics and Spectroscopy by Stimulated Emission Pumping*, edited by H. L. Dai and R. W. Field (World Scientific, Singapore, 1995).

[4] S. Guérin and H. Jauslin, Eur. Phys. J. D **2**, 99 (1998).

[5] M. V. Danileiko, V. I. Romanenko, and L. P. Yatsenko, Opt. Commun. **109**, 462 (1994).

[6] J. Martin, B. W. Shore, and K. Bergmann, Phys. Rev. A **52**, 583 (1995).

[7] J. Martin, B. W. Shore, and K. Bergmann, Phys. Rev. A **54**, 1556 (1996).

[8] A. Kuhn, S. Schiemann, G. Z. He, G. Coulston, W. S. Warren, and K. Bergmann, J. Chem. Phys. **96**, 4215 (1992).